Effect of Flow Induced Parameters on the Output of A High Repetition Rate Dye Laser

Rajeev Chaube (rchaube@rrcat.gov.in)
Raja Rammana Centre for Advanced Technology

Research Article

Keywords: dye laser, gain medium inhomogeneities, fluid structure interaction, flow cell, CFD.

Posted Date: December 14th, 2021

DOI: https://doi.org/10.21203/rs.3.rs-1136907/v1

Effect of flow induced parameters on the output of a high repetition rate dye laser

(Rajeev Chaube)

Design Manufacturing and Technology Division,

Raja Ramanna Centre for Advanced Technology

Indore ¯ 452013 (India)

e-mail: rchaube@rrcat.gov.in

Fax: 91-0731-2442290

Phone: 91-0731-2488713

Abstract:

The factors influencing the optical path stability in a dye laser flow cell are studied numerically and experimentally. A specially designed curved metallic dye flow cell providing a gain medium of 25 mm x 0.5 mm x 0.2 mm along with a compact resonator mechanical assembly is used in the study. The same configuration with gain medium of 15 mm x 0.5 mm x 0.2 mm is successfully used for single mode dye laser. The effects of flow induced vibrations on dye flow cell are studied with and without mechanically coupling it with the resonator structure for flow speeds varying from 1.33 m/s to 6.67 m/s at laser pump position. The effect of the mechanical instability, velocity fluctuation and temperature fluctuations in flowing dye solution on dye laser performance are studied at different flow speeds. These results are compared with the dye laser output parameters and found to be in good agreement. This study is useful in designing a high stability narrowband dye laser.

Key words: dye laser, gain medium inhomogeneities, fluid structure interaction, flow cell, CFD.

1. Introduction:

Tuneable dye laser with narrow frequency line width pumped by high repetition rate high power copper vapour laser (CVL) or its advanced variants are mostly used in material processing, laser isotope separation [1, 2], medicine [3, 4], high resolution spectroscopy [5, 6] and many other applications. A dye laser is an integrated assembly of pump laser, resonator and dye flow cell. Among these the dye flow cell mostly governs the associated functional parameters with a dynamic system that can be rearranged by varying flow inlet conditions, flow rate, solvent composition, dye concentration etc. The flowing organic dye solution sets the lasing wavelength by managing the optical gain. The fluctuations in optical path within laser resonator influence the emission line width of dye laser radiation. These fluctuations are caused by pump power variations, mechanical instabilities, velocity fluctuations in flowing dye solution and direct dye solution temperature fluctuations due to heat deposition by pump laser [7]. As a result the intensities of simultaneously oscillating modes and gain relations alter due to the fluctuation of the coupling strength between modes. The wide bandwidth of the gain medium, along with the mechanical unsteadiness of speedily flowing dye solution results in frequency selection and stabilization a difficult task. The frequency stability of dye laser is often determined by mechanical stability of the optical elements, the flow and thermal behaviour of the gain medium and resonators superstructure.

While the influence of velocity fluctuation and dye solution temperature fluctuation on fluctuation in the optical path within laser resonator is reported in the literature [8, 9, 10], the effect of flow induced vibration on mechanical instabilities of dye laser setup is not yet reported in detail. An unperturbed optical layout provides good frequency stability, but there are some practical limitations. Flow induced vibrations changes the optical path in flow cell and may also excite fundamental mechanical resonances. These high frequency vibrations (In range of 100 ¯ 1000 Hz) are often reduced by mounting the system on shock absorbing materials and passive masses [11]. Vibration isolation table generally take care of low frequency vibrations from ground noise and building vibrations.

The pulsed CVL beam deposits the heat on dye laser window which is absorbed by flowing dye medium. This leads to change in refractive index due to temperature gradient which finally results in variation of wave length in dye laser [12, 13]. To take off the gain medium heated by every CVL pulse, the speed of the fluid across the axis of the dye laser is often magnified by narrowing the flow channel. This results in the reduction of the geometrical hydraulic parameters of dye flow cell at CVL pump region [1, 14, 15]. As a result the non uniform thermal and flow eddies/ inhomogeneities are created. This result in non-uniformities in refractive index of the flowing dye gain medium and unfavourably influence the output of the dye laser. Moreover the high solvent flow velocity leads to the scattering centres due to cavitations depending on dye flow cell geometry and thermal properties of solvent being used [16, 17]. Absence of stream wise recirculation zone allows very few distortions of the wave front of the dye laser beam [18]. A careful design of dye flow cell and predicting its hydrodynamic performance along with dye laser parameters is therefore useful. When the flow field and temperature field are homogeneous the entire gain medium can put in power to the oscillating laser mode. With inhomogeneous flow and temperature field the emission band of a specific group of excited molecules is different from the emission spectrum of the system as a whole. There exists temperature gradient/difference between downstream and upstream relative to pump laser CVL impact position in a dye cell due to the heat deposited by each pulse. This was studied by Amit et al by analyzing He Ne beam deflection and spread [8]. They used dye solution having 10% ethylene glycol in methanol and through a flow passage of 0.5 mm for the flow rate between 0.3 lit/min to 5 lit/min. A dye cell having 20 mm gain length was used by Maruyama et al and they found that flow speed of dye solution in the dye cell to be about 5 m/s is adequate for downright re substitution of exited dye solution between consecutive pulses of pump laser [5]. They also discussed a dye laser with gain length of 8 mm and with flow speed between 0.6 m/s to 8 m/s and ascertained frequency jitter because of turbulence at higher flow [19].

In this article we present our experimental and analytical study on the essential

parameters that influence the dye laser stability. A specifically designed dye laser set up was successfully used in a control experiment to relate the parameters influencing the dye laser performance. The main conclusion in this work is that the flow induced vibrations and associated mechanical instabilities, flow field behaviour and temperature field behaviour are strongly correlated to the dye laser performance. We examine each of these critical parameters independently in our specially designed dye laser set up and discuss the improvements associated to achieve high quality performance of dye laser collectively.

2. Dye Laser setup:

We have used an inexpensive in-house designed and fabricated arrangement to accommodate optical components and dye cell in a single mechanical structure that may compensate for the environmental effects [9]. The dye flow cell providing dimension of dye gain medium to be 0.2 mm x 0.5 mm x 25 mm was united in a mechanical assembly having provision to accommodate the required optics. In front of the dye cell, a cylindrical lens holder was mounted. This holder has a feature to rotate the cylindrical lens which helps in aligning the pump beam with the dye laser axis. Copper vapour laser beam was focused on to the dye medium using a cylindrical lens of focal length 55 mm. The optical layout of dye laser used is shown in figure 1.

It is fundamentally a traditional grazing incidence grating (GIG) arrangement [20, 21]. Dye laser optical configuration is housed in a single mechanical structure which has been in house fabricated [9]. In this mechanical structure the laser axis was folded at right angle with the help of a beam expander prism of magnification of about 8.5 which is anti reflection coated for 570-590 nm. The dye laser beam was expanded by the prism and folded by 90^0 before incidence on a nearly placed grating with 2400 lines opposite to a tuning mirror and an output coupler having 20 % reflectivity. The dye laser beam output parameters were analyzed using a Fabry-Perot etalon of finesse = 25 and FSR = 5 GHz. A CCD camera was also linked to a computer. As a reference laser a He-Ne laser beam ($\lambda = 632.816$ nm) with frequency stabilization was arranged to travel through the optical path of the dye laser beam. As the complete dye laser set up is accommodated in a single mechanical structure, the

effect of environmental thermal effects and induced vibration and are significantly decreased due to high stiffness of this mechanical structure. The dye flow solution was prepared of a mixture of 30%, ethanol and 70% glycol with 1 mM concentration of Rhodamine 6G in. The dye flow cell was connected to a Stainless Steel (SS) pump, valves, a large SS reservoir, flow meter, micron filter and a compacted chiller unit of rating 1.5 TR.

To house the entire resonator optical layout a specially designed single monoblock metallic structure was employed [9]. In this monoblock resonator structure the grating mount has arrangements for changing the grating angle and alignment of the grating grooves at right angles to the incident beam. In order to accurately position it at necessary angle on the dye cell-grating axis, the beam expander prism could be translated and rotated. The tuning mirror has provision for tilting it in the vertical plane. The cylindrical lens for focusing the pump beam was placed in a mount that has arrangement for linearly moving it with respect to the dye cell for optimising the focusing conditions. It could also be rotated for angular adjustment of the pump region. All the individual optical mounts, made of stainless steel 304, were supported on two guide rods and bolted on to the two sides of the dye cell to form a single monolithic block. The self-weight of this monoblock makes it immune to the external vibrations caused by flow. Such a high mass also ensures that changes in resonator length, because of expansion of optical mounts due to the environmental temperature changes, will be on longer time scale.

3. Experimental set up for estimation of flow induced mechanical instabilities (figure 2):

In order to conduct experiments to evaluate flow induced mechanical instabilities a prototype dye cell with all the dimensions similar to actual dye cell was fabricated. This test cell differs with actual dye flow cell only in side flat walls which are made of transparent acrylic glass in place of SS material. An observational experimental set up is briefly described as follows. A test cell with geometry similar to the dye laser mechanical structure but instead of SS for end flat walls transparent acrylic glass was used for this experiment. This was done to perform experiments at different flow

positions. A mixture of 30% ethanol and 70% glycol which is the solvent used in dye laser experiments was made to circulate in test dye flow cell. In order to ensure temperature variation in extended time scale, the test cell was coupled to a large capacity SS reservoir with high pressure SS pump, flow regulating valves, micron sieve, magnetic flow meter ($^{+}$/- 2% accuracy of full flow), gauge to measure pressure difference, compacted chiller unit 1.5 TR ($^{+}$ /- 0.1 ^{0}C stability) and a temperature monitor ($^{+}$/- 0.1^{0}C accuracy).

A 2 mW He-Ne laser beam (632.8 nm) with about 2.25 m rad. divergence was made to fall on the test flow cell using appropriate natural density optical filters as attenuators at 180^{0} location which is laser pump position. The He-Ne laser light beam coming out from test flow cell was arranged to fall on a CCD window (PCO Pixel Fly camera PCO AG). This camera has facility to select acquiring time and pixel size. A frame grabber interface was used to connect CCD to a computer. The beam passed on through the flowing medium resulted in intensity distribution and spatial shift which were captured in the computer. Each consecutive image of line profile of intensity distribution and spatial shift was automatically stored in a computer and compound images were analyzed. Image processing software which was developed in-house was used in this experiment [22]. This software automatically obtains the intensity profile with spatial shift and constitutes pictures of the data composed from all frames over a given time period. The greatest eddy turn over time for the given flow conditions was calculated and the CCD acquiring time was set accordingly. It was estimated that 150 frames each were adequate to analyze results [17].

4. Numerical scheme for evaluation of flow inhomogenieties and temperature inhomogenieties:

All numerical Fluid Structure Interaction (FSI) modeling packages use Reynolds Averaged Navier-Stokes (RANS) to resolve a flow field. Though these methods are economical, they can˘t convey the time-coherent pressure variations at the wall of the apparatus that are the driving mechanism of turbulence-induced vibration. For a fully developed turbulent flow in a closed channel the velocity distribution is closely approximated by seventh root low [23]. When the amplitude of flow induced

vibration increases the mean velocity profile in flow duct gets modified and is different from those approximated by seventh root low or obtained by solving RANS [24]. Large Eddy Simulation (LES) solves for a local-averaged velocity rather than a time-averaged velocity to produce the pressure variations resulting the flow vibrations. Therefore, coupling an LES-based fluid model with a structural model that provides the capability necessary to analyze the turbulent-induced phenomenon has been used.

The CVL spot size ($= f \times \theta$) is estimated to be about 200 microns, for about 3 m rad divergence. Using a 5 cm focal length cylindrical lens the CVL ($\lambda = 510nm$) with beam size (*D*) of 25 mm was line focused on the optical window of dye laser. Therefore the CVL heat flux falling on the 25 mm x 0.2 mm area at CVL impact or pump position which is 180^0 angular position. For simulation the heat flux calculated for 5 W CVL was applied on CVL impact position i.e 180^0 angular position. The CVL inter pulse duration is 200 microsecond when operating at 5 KHz. Following the Beer-Lamber law the depth of penetration of pump beam in the dye medium will be about 100 microns. Under these conditions, for successful inter pulse volume replacement at CVL impact position the minimum flow velocity required will be about 0.67 m/s. In the dye gain medium the temperature gradients were simulated by varying flow speed at CVL impact position from 0.67 m/s to 6.67m/s to cover a broad range of clearing ratio. The pressure fluctuations in dye flow cell are obtained using Large Eddy simulation for different flow rates at different pump speeds.

5. Results and discussions:

5.1 Dye Laser Output: Figure (3) shows photograph of dye laser output Fabry-Perot fringes. For camera exposure time of about 40 ms these are the superposition of about 100 dye laser pulses [25].

To record and capture the fringes a frame grabber card with CCD camera was used. Additionally software that estimates variation of the bandwidth and wavelength from the record of fringes was used [22]. As may be seen from figure (3) three axial modes appear with bandwidth of individual mode about 300MHz. The estimated resonator length is about 15.89 cm and the estimated frequency for this resonator length is about

935 MHz. It was observed that among three oscillating modes, two adjacent modes compete for the gain with varying intensity. Additionally long term stability in the

fringe pattern was recorded It was also seen that the axial modes separates by about 990 MHz which is nearly same i.e. about 935 Mhz as the value calculated for the given resonator length. We have earlier shown the dependence of dye laser output parameters on dye solution flow field fluctuations and temperature fluctuations using curved dye cell [13, 17]. The band width varied from 2.4 GHz to 324.3 MHz and wave length varied in a narrow range depending on the flow conditions. In present study we have shown the dependence output parameters of dye laser on flow induced mechanical instabilities apart from flow field fluctuations and temperature fluctuations. At a flow speed of about 7.33 m/s the bandwidth varied from 235 MHz to 324 MHz and the wavelength corresponding to the central mode varied from 576.228 to 576.2289 nm. Dye flow rate was varied to see the effect of flow rate on the stability of the dye laser output [25]. When flow speed was reduced from 7.33 m/s to 5 m/s the variation in wavelength and the bandwidth increased from 575.999 to 576.991 nm and from 446 MHz to 598 MHz respectively. When flow speed was further reduced from 5 m/s to 1.6 m/s the variation in wavelength and the bandwidth further increased from 575.999 to 576.991 nm and from 392 MHz to 624 MHz respectively.

The same design of the dye laser set up with gain medium dimension 0.2 mm x 0.5 mm x 25 mm was used in single mode operation [26]. The dye solution now was prepared of Rhodamine 6G (2 mM concentration) in the ethanol. A wave-meter (WS-7, Angstrom, High Finesse) was used to study the dye laser wavelength and band width. In single mode operation dye laser wavelength the flow speed was optimized at 6.5 m/s. Figure 4 shows the results at optimized flow speed of 6.5 m/s. The wavelength varied from 587.13980 nm to 587.14010 nm and bandwidth remained constant at 0.1 pm (± 88 MHz).

5.2 Flow induced mechanical instability:

As shown in figure 5 the coupling of the dye flow cell of mass m_1 and stiffness k_1 with the mono block dye laser resonator assembly of mass m_2 and stiffness k_2 acts as tuned vibration absorber for dye flow cell.

If dye flow cell is subjected to flow induced force $F \operatorname{Sin} \omega t$ the system will have a steady state response given by $x = \frac{F \operatorname{Sin} \omega t}{m\left(\omega_n^2 - \omega^2\right)}$ (1),

where ω_n is the natural frequency of dye cell and is given by $\omega_n = \sqrt{\frac{k_1}{m_1}}$ (2)

and x is maximum when $\omega = \omega_n$ [27, 28]. The equation of motion for this system is given by

$$\begin{bmatrix} m_1 & 0 \\ 0 & m_2 \end{bmatrix} \begin{pmatrix} \ddot{x}_1 \\ \ddot{x}_2 \end{pmatrix} + \begin{bmatrix} k_1 + k_2 & -k_2 \\ -k_2 & k_2 \end{bmatrix} \begin{pmatrix} x_1 \\ x_2 \end{pmatrix} = \begin{pmatrix} F \operatorname{Sin} \omega t \\ 0 \end{pmatrix} \qquad (3)$$

Where x is the displacement

The solution to this equation gives amplitude as

$$X_1 = \frac{\left(k_2 - m_2\omega^2\right)F}{k_1k_2 - m_1k_2\omega^2 - m_2k_1\omega^2 - m_2k_2\omega^2 + m_1m_2\omega^4} \qquad (4)$$

$$X_2 = \frac{-k_2F}{k_1k_2 - m_1k_2\omega^2 - m_2k_1\omega^2 - m_2k_2\omega^2 + m_1m_2\omega^4} \qquad (5)$$

From equation (4) it is clear that $X_1 = 0$ when $\omega^2 = \frac{k_2}{m_2}$. Therefore if the resonator structure is suitably designed with proper choice of stiffness (k_2) and mass (m_2) and coupled with the dye flow cell of stiffness (k_1) and mass (m_1), the vibrations may be completely eliminated or reduced to the extent of elimination from dye flow cell.

Figure 6 and figure 7 shows the pattern of turbulence in dye cell in the form of comprehensive pictures of intensity contours obtained by CCD. Figure 6 shows the observations in prototype test dye cell at different flow speed and figure 7 shows the

observations in prototype test dye cell that is coupled to a heavy mono block resonator assembly for different flow speed. From the calculated maximum time period of turbulent eddy ($t = l / V$) it was estimated that 150 frames per observation are sufficient to adequately capture the centroidal motion of the beam. While column (a) represent intensity variation of He Ne beam transmitted through test cell, column (b) represents shifts in radial peak positions of intensity and column (c) is collective picture of both. The erratic pattern of intensity contours shown in column (a) and (b) exhibit the time averaged fluctuating velocity components that results in Reynolds or turbulent stresses. It is clear that in both the cases the RMS values of intensity variation and radial shift in peak position of intensity decreases with increase in flow rate. The RMS value of intensity variation and radial shift in peak position reduces from 108 and 63 to 54.44 and 24 when test dye cell is independently tested and flow velocity at pump position of dye cell is varied from 1.33 m/s (Re =183) to 6.67 m/s (Re =915). The RMS value of intensity variation and radial shift in peak position reduces from 65 and 27 to 21 and 12 when test dye cell is coupled with the resonator structure and flow velocity at pump position of dye cell is varied from 1.33 m/s (Re =183) to 6.67 m/s (Re =915). Thus when the dye flow cell is mechanically made to be a part of resonator structure, the influence of flow induced vibrations in dye flow cell are significantly reduced.

5.3 Flow inhomogenieties (velocity fluctuations):

A clearing ratio resulting from flow velocity of about 4 m/s at CVL pump position in dye flow cell is usually optimum and mostly used. This corresponds to Reynolds number 550 at CVL pump position is and is chosen for subsequent numerical analysis on flow induced inhomogeneities. For Reynolds number of 550 as may be seen from figure 8 that the stream wise recirculation zone that may cause the distortions of the wave front of the dye laser are not present at laser pump position.

The vector representation of cross flow velocities at CVL impact position is shown in figure 9a, (scaled on 0.5 mm gap) with arrow length representing the relative magnitude. The resulting instantaneous flow inhomogeniety is shown in

figure 9b.

It may be seen that at the place of lowest hydraulic diameter (or gap) all along the flow path the swirls are more powerful in magnitude at outer wall (CVL impact position) than that at inner curved wall. These swirls are responsible for the transportation of deposited heat from outer wall (CVL impact position) to the core of the fluid flow at still low Reynolds Number. Infect this is a crucial prerequisite while designing dye laser system for high power. However these whirls augment the inhomogeneities in dye gain medium. The flow and the resulting thermal field are the sum of mean ($\overline{V}$, $\overline{T}$) and erratic (V' , T') motion as given below [9, 17, 29]:

$$V = \overline{V} + V' \text{ and } T = \overline{T} + T' \qquad (6)$$

A laser beam passing through the flow or temperature inhomogeneity of varying length scale will undergo the variation in output [30, 31]. The flow inhomogeneity scale length varies from size of hydraulic diameter to turbulent scale length. These inhomogeneity scale length were numerically calculated at CVL pump position by dividing flow area in 10 x 10 lattices. At each lattice point the flow kinetic energy (k) and its dissipation rate (ε) was calculated numerically. At all 100 lattice points the inhomogeneity scale lengths were calculated for flow field at CVL pump position ($l = \frac{k^{3/2}}{\varepsilon}$). The deviation in the inhomogeneity scale length was calculated as $l_{\text{var}} = \frac{l_{\max} - l_{\min}}{l_{\max}}$.

The estimated size of flow field inhomogeneity reduced from 8 μm to 1.84 μm on increasing the flow speed from 1.34 m/s to 6.67 m/s.

5.4 Temperature inhomogenieties (Temperature fluctuations):

Pulsed laser input of 200 μsec inter pulse duration and 40 nsec pulse width is applied to the CFD model for bulk flow velocity of 4 m/s at CVL impact position.

The temperature rise in dye gain medium at CVL pump position (180^0 angular position) with each pulse is shown in figure 10a and resulting instantanious

temperature inhomogeiniety is shown in figure10b.

These are the contours of potential temperatures which are the summation of mean temperature and its fluctuating component ($T = \overline{T} + T'$). The temperature fluctuation associated with inhomoginity of size *l* is given as

$$T'^2 \sim \frac{N_T l^{2/3}}{\varepsilon^{1/3}}$$

Where N_T is the dissipation rate of the fluctuation of scalar T'.

For numerically calculating the variation of temperature inhomogeneity, the zone of the thermal boundary layer in the flow field at CVL impact position was divided by $10\,\mu m$ intervals. Subsequently the variation in the average temperature inhomogeneity within thermal boundary layer was calculated as $T_{var} = \frac{T_{max} - T_{min}}{T_{max}}$.

The estimated variation in temperature field reduced from 1.92^0C to 0.48^0C on increasing the flow speed from 1.34 m/s to 6.67 m/s. The variation in temperature inhomogeneity at different flow speed is discussed with dye laser parameters in section 4.

5.5 Comparison of flow induced parameters with dye laser output:

In a CVL the pulse to pulse divergence and hence energy per pulse does not change noticeably because of fixed distance between resonator mirrors and fixed discharge tube diameter. Thus the CVL power pumped to dye laser will not change from pulse to pulse. Therefore for the dye laser set up presented here, the dye laser output parameters will be solely dependent on the mechanical instability, fluctuations in velocity and dye solution temperature. These 3 parameters are directly linked with the flow induced vibrations in the dye flow cell.

Figure 11 shows the comparison of flow induced parameters with dye laser band width and wave length from 60 min of observation time. All the values are

normalized to compare on the same scale. As the thermal and flow inhomogeneities decreases by increasing bulk flow velocity of dye solution the variation in optical path length in dye medium also decreases. This explains the reliance of band width and wave length variation on duct geometry, flow and thermal character of flowing medium in the duct. Additionally the dye laser output parameters are correlated with the mechanical instability of the test dye flow cell which is mechanically integrated to the resonator monoblock structure figure (11). It is shown in section 5.2 that there is a significant reduction in flow induced turbulence and mechanical instability of dye flow cell when it is mechanically coupled with the massive resonator structure.

6. Conclusions: The parameters adversely effecting dye laser performance caused by mechanical instabilities, velocity fluctuations in flowing dye solution, variations in laser pump power and direct dye solution temperature fluctuations due to heat deposition are studied experimentally and numerically using an experimental dye flow test cell. These experimental and numerical results are compared with dye laser output parameters. A specially designed dye flow cell and its laser resonator are discussed with the influence of this design on dye laser output parameters. The same configuration was also used for single mode dye laser and gave almost constant band width. It is shown that curved dye flow cell with its concave wall facing incident pump laser beam enhances the heat transfer to the core flow even at low flow velocity. It is also analytically and experimentally shown that if the dye flow cell is coupled to a suitably designed massive resonator structure the influence of flow induced vibrations or mechanical instabilities in dye flow cell may be significantly reduced. The stream wise recirculation zones that may cause the distortions of the wave front of the dye laser are eliminated in this design.

References:

[1] R P Hackel 1993 *SPIE Laser Isotope Separation* **1859** 120-128.

[2] J A Paisner 1988 *Applied Physics B* 46 253 ¯ 260

[3] L Goldman 1990 Dye laser in medicine in *Dye Laser Principles, (*F. J., Duarte and L. W. Hillman, Eds. Academic Press New York Chap 10) 419¯432

[4] F J Durate and L W Hillman 1990 *Dye Laser Principle with applications* (Academic Press, New York) 254-256

[5] Y Maruyama, M Kato, T Arisawa 1996 *Optical Engineering* **35**(4) 1084 ¯ 1087

[6] G A Capelle, J P Young, D L Donohue and D H Smith 1987 *J. Opt. Soc. Am B* **4**(4) 445-451

[7] H W Schroder, Welling H and Wellegehausen B 1973 *Appl. Phys.* **1** 343-348

[8] M Amit, G Bialolenker and D Levron 1988 *J. Appl. Phys* **63**(5), 1293-1298

[9] R Chaube 2008 *Optical Engineering* **47**(1) 014301-(1-7)

[10] V S Rawat, L M Gantayet, G Sridhar and S Singh 2014 *Laser phys* **24**

[11] J C Bergquist, W M Itano and D J Wineland 1992 Laser stabilization to a single ion: Proc of the international school of physics, North Holland, Amsterdam, 359-376

[12] C S Zoe 1984 *Applied Optics* **23** (17), 2879-2885

[13] R Bhatnagar, R Chaube and N Singh 2005 *Applied Optics* **44** (32) 6962 ¯ 6970

[14] A F Bernhardt 1981 *Applied Physics* **B26** 141-143

[15] M D Ainsworth, A C J Glover, and J A Piper 1995 *Applied Optics* **34**(27), 6108 ¯ 6113

[16] SG Varnado 1973 *J Appl Phys* **44** (11) 5067-5068

[17] R Chaube 2010 *Optics & Laser Technology* **42** 819¯827

[18] D Doize, L A Lompre and P Arondel 1993 Dye laser chain for laser isotope separation : Proc of the international symposium on advanced nuclear energy research 179-185

[19] Y Maruyama, M Kato, T Arisawa *Optics Communication* **81**(12) 67 ¯ 70

[20] M G Littman 1978 *Opt. Lett*. **3** 138¯140

[21] F J Duarte and J A Piper 1981 *Applied Optics* **20** (12) 2113-2116

[22] H S Vora, N Singh and R Bhatnagar 2002 Proc of the National Laser Symposium India

[23] S Norma, Y Sasaki and K Murakami 2000 *Jpn. J. Appl. Phys* **39** 4987-4989

[24] S Y Kin, X Bonnardel, J P Guilergia, E Brocher, 1994 *Smart Mater Struct*. **3**, 6-12,

[25] N Singh, R Chaube, H S Vora, R Bhatnagar, 2004, *CAT internal report*, CAT/2003-29

[26] O Prakash, J Kumar, R Mahakud, P Saxena, V K Dubey, S K Dixit, J K Mittal, 2011, *Optics & Laser Technology,* **43**, 1475¯1481.

[27] W T Thomson 1988 *Theory of vibration with application* (4th edition, Prentice Hall, a Simon Schuster Company) 143-145,

[28] J K Vandiver 2012 *Journal of Fluids and Structures* **35** 105¯119

[29] R Chaube 2015 International Journal of Fluid Mechanics Research **42**(1) 39-58

[30] V I Tatarshii *Physics of fluctuations of waves in turbulent medium* http://home.comcast.net/~v.tatarskii/vit.htm

[31] R Chaube 2015 *Optik- Int. J. Light Electron Opt.* **126** 759¯764

Funding: The author declares that no funds, grants, or other support were received during the preparation of this manuscript.

List of figure captions:

Figure 1 Optical layout of dye laser system

Figure 2 Experimental set up for comparing turbulence in dye laser test cell at different flow rates

Figure 3 Fabry-Perot (FSR 5 Ghz) rings of dye laser

Figure 4 Single mode dye laser variation of wavelength and bandwidth with time.

Figure 5 Symbolic mechanical assembly of resonator with dye flow cell housed in it.

Figure 6 Turbulence pattern at laser pump position in test dye flow cell as intensity variation of He Ne beam transmitted through prototype test cell and radial shifts in peak positions of intensity for sum flow velocities and Reynolds number 1.33 m/s and 6.67m/s when test dye flow cell is not coupled to the resonator structure.

Figure 7 Turbulence pattern at laser pump position in test dye flow cell as intensity variation of He Ne beam transmitted through prototype test cell and radial shifts in peak positions of intensity for sum flow velocities and Reynolds number 1.33 m/s and 6.67m/s when test dye flow cell is coupled to the resonator structure.

Figure 8 Stream wise sum velocity vector at Re = 550 in dye flow cell.

Figure 9 (a) Cross flow velocity vector and (b) resulting flow inhomogeneity at Re = 550 in dye flow cell at laser pump position

Figure 10 (a) Instantaneous temperature rise in dye gain medium with each pulse and (b) resulting temperature inhomogeiniety

Figure 11 Variation of different parameters from test dye flow cell and comparison with dye laser output at different flow velocities at laser pump region.

Figures

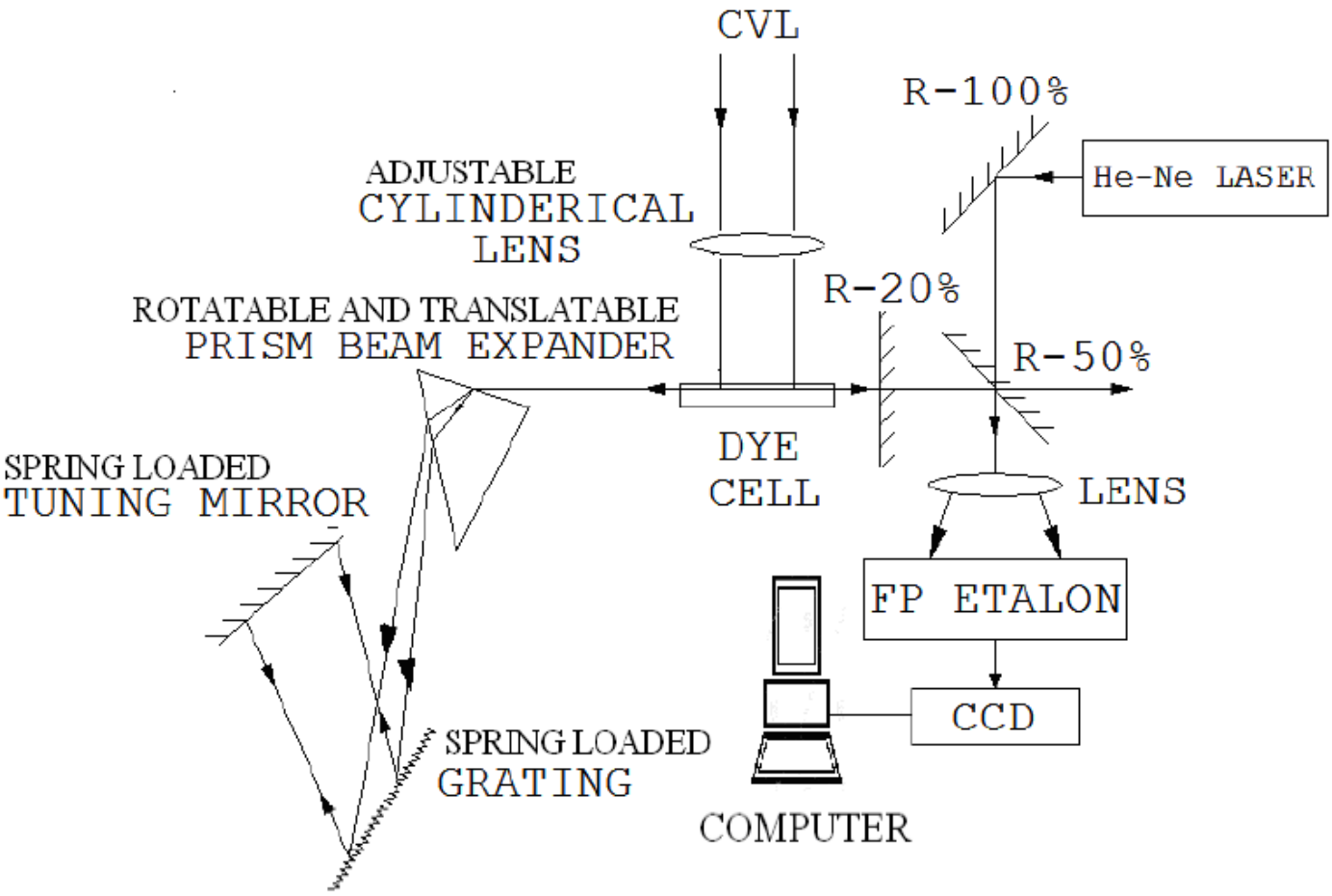

Figure 1

Optical layout of dye laser system

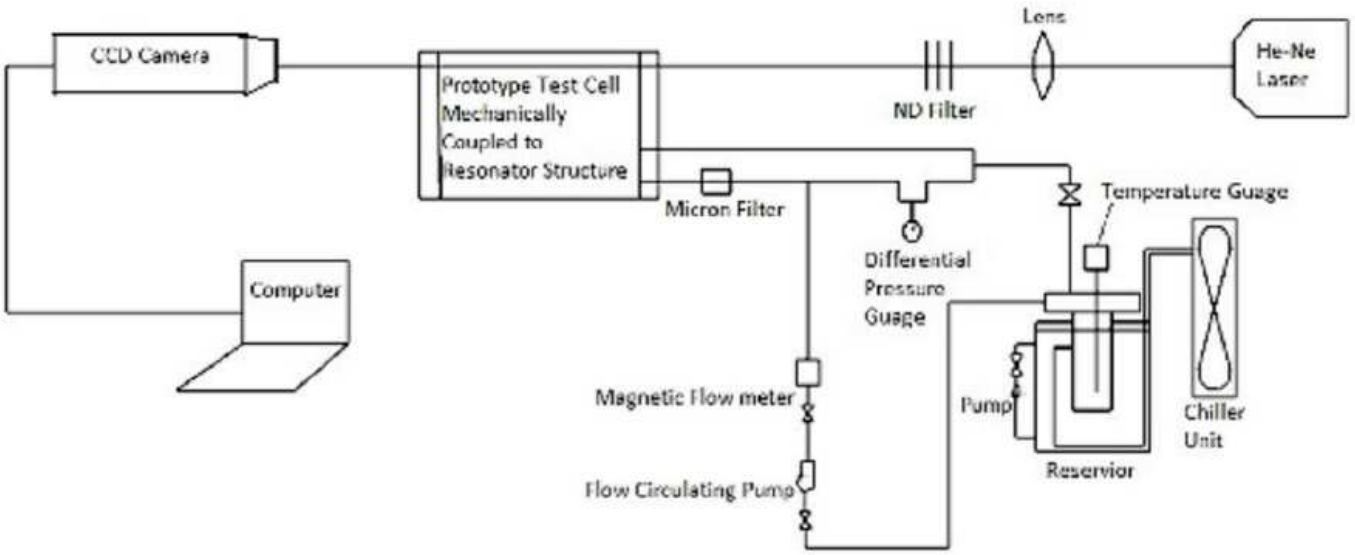

Figure 2

Experimental set up for comparing turbulence in dye laser test cell at different flow rates

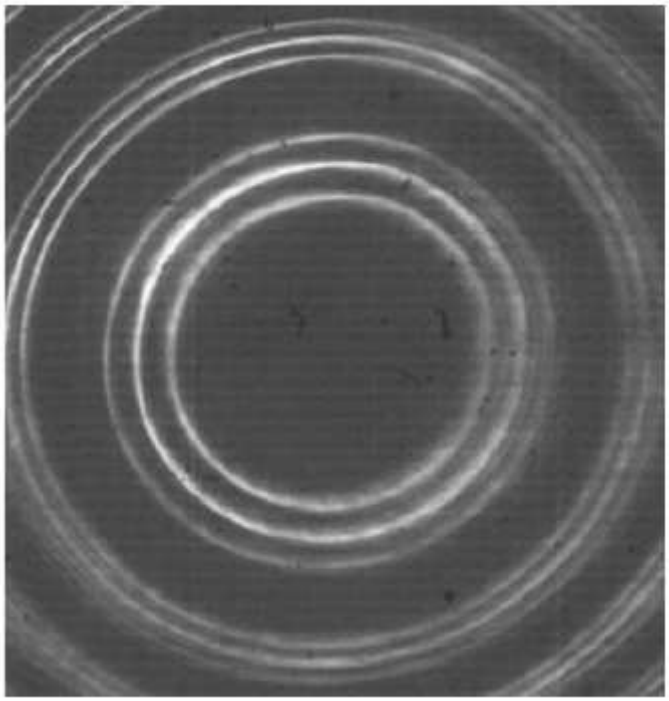

Figure 3

Fabry-Perot (FSR 5 Ghz) rings of dye laser

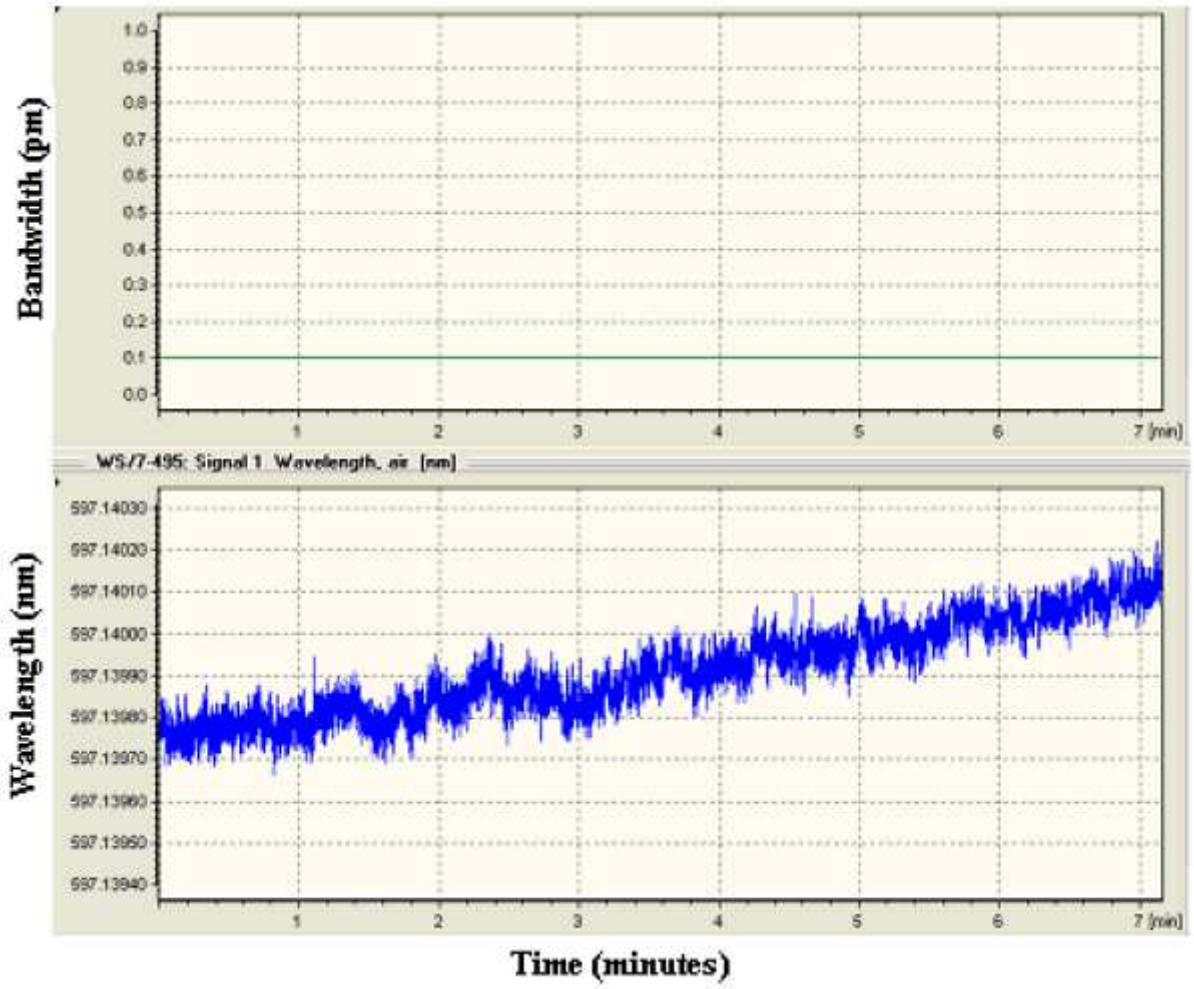

Figure 4

Single mode dye laser variation of wavelength and bandwidth with time.

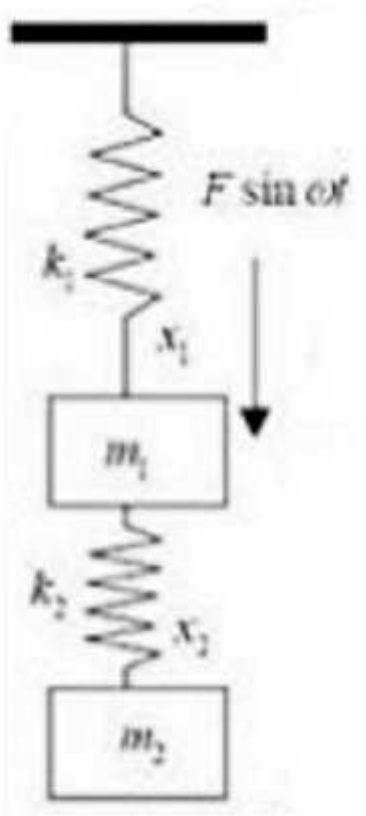

Figure 5

Symbolic mechanical assembly of resonator with dye flow cell housed in it.

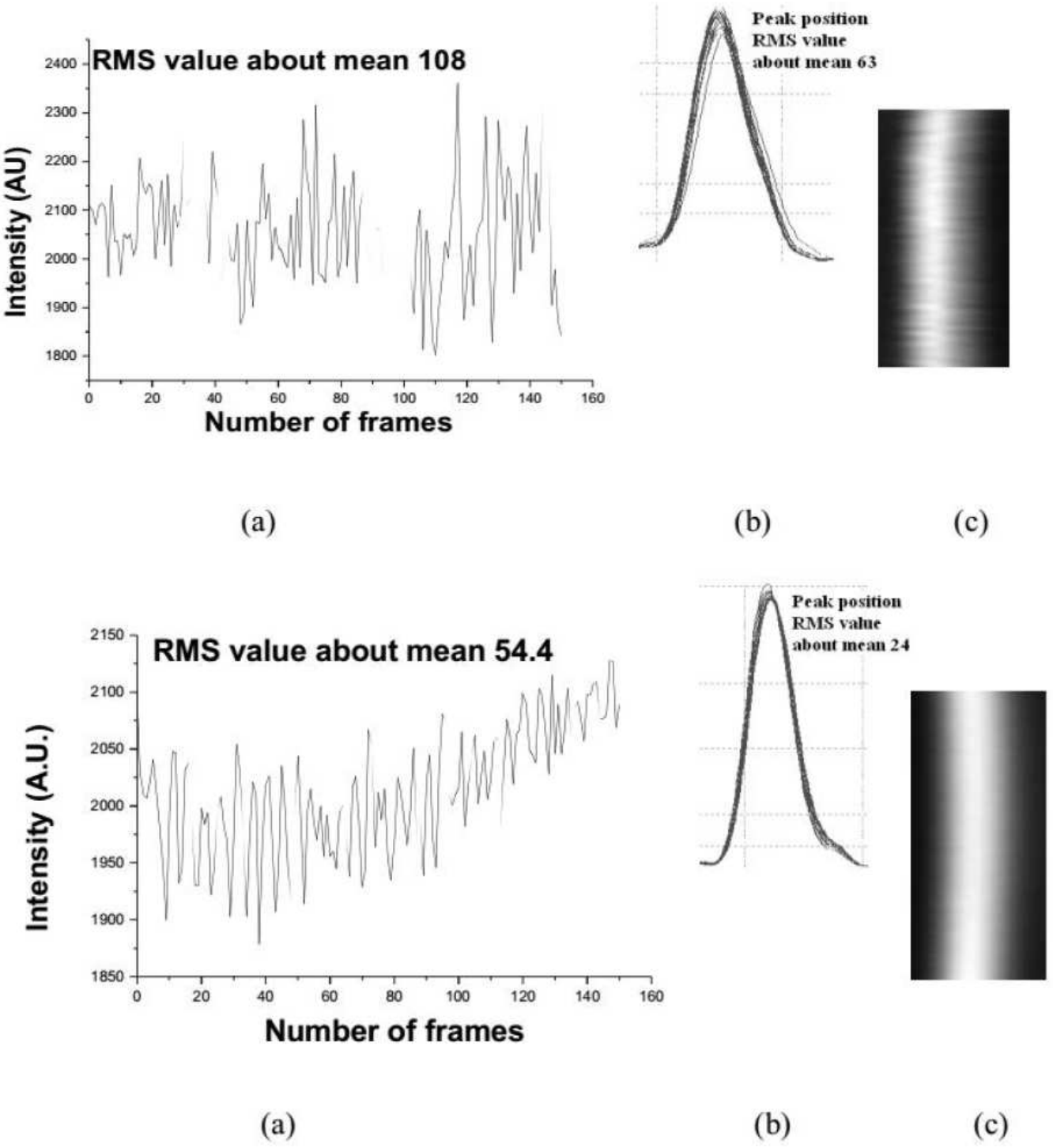

Figure 6

Turbulence pattern at laser pump position in test dye flow cell as intensity variation of He Ne beam transmitted through prototype test cell and radial shifts in peak positions of intensity for sum flow velocities and Reynolds number 1.33 m/s and 6.67m/s when test dye flow cell is not coupled to the resonator structure.

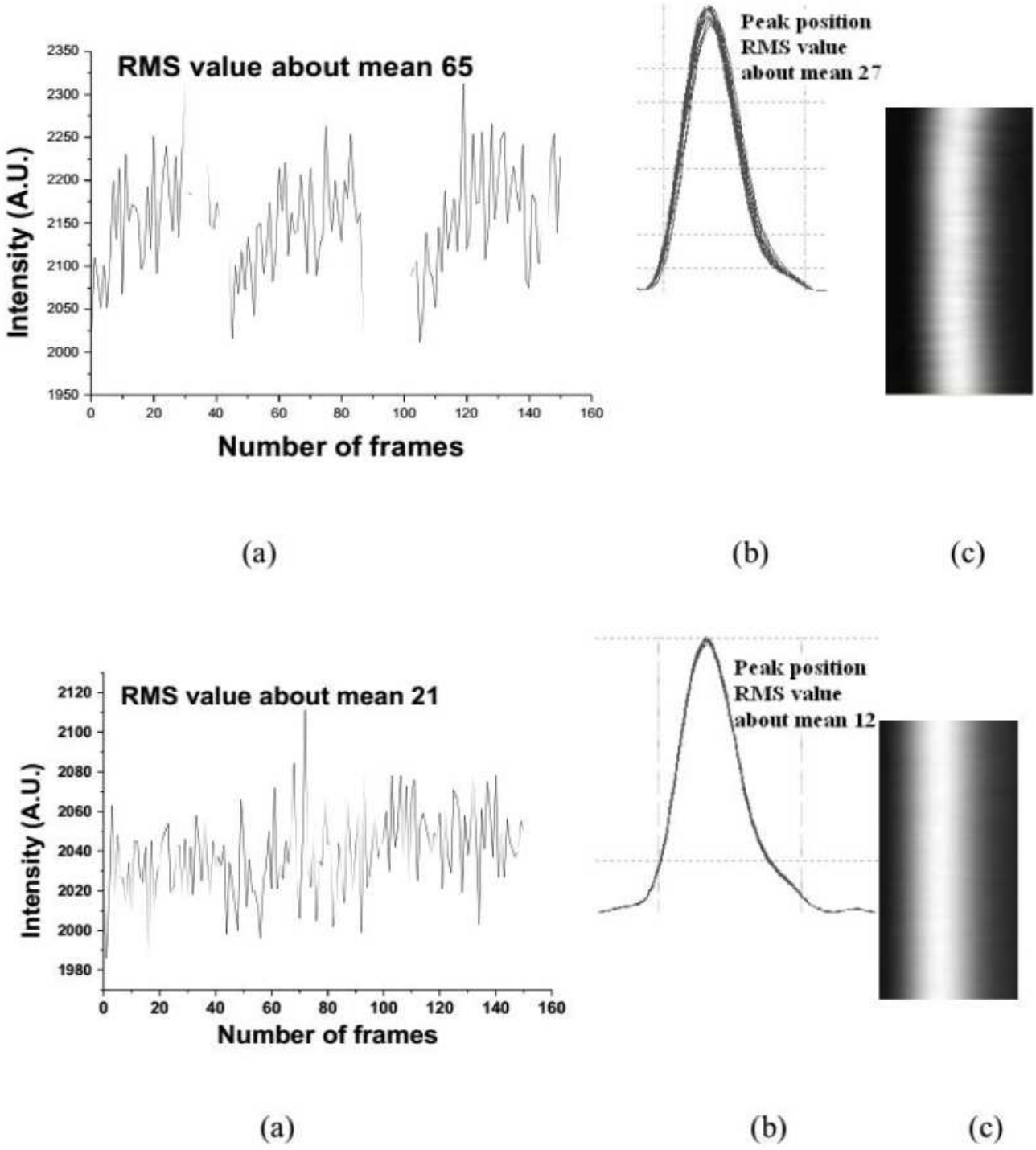

Figure 7

Turbulence pattern at laser pump position in test dye flow cell as intensity variation of He Ne beam transmitted through prototype test cell and radial shifts in peak positions of intensity for sum flow velocities and Reynolds number 1.33 m/s and 6.67m/s when test dye flow cell is coupled to the resonator structure.

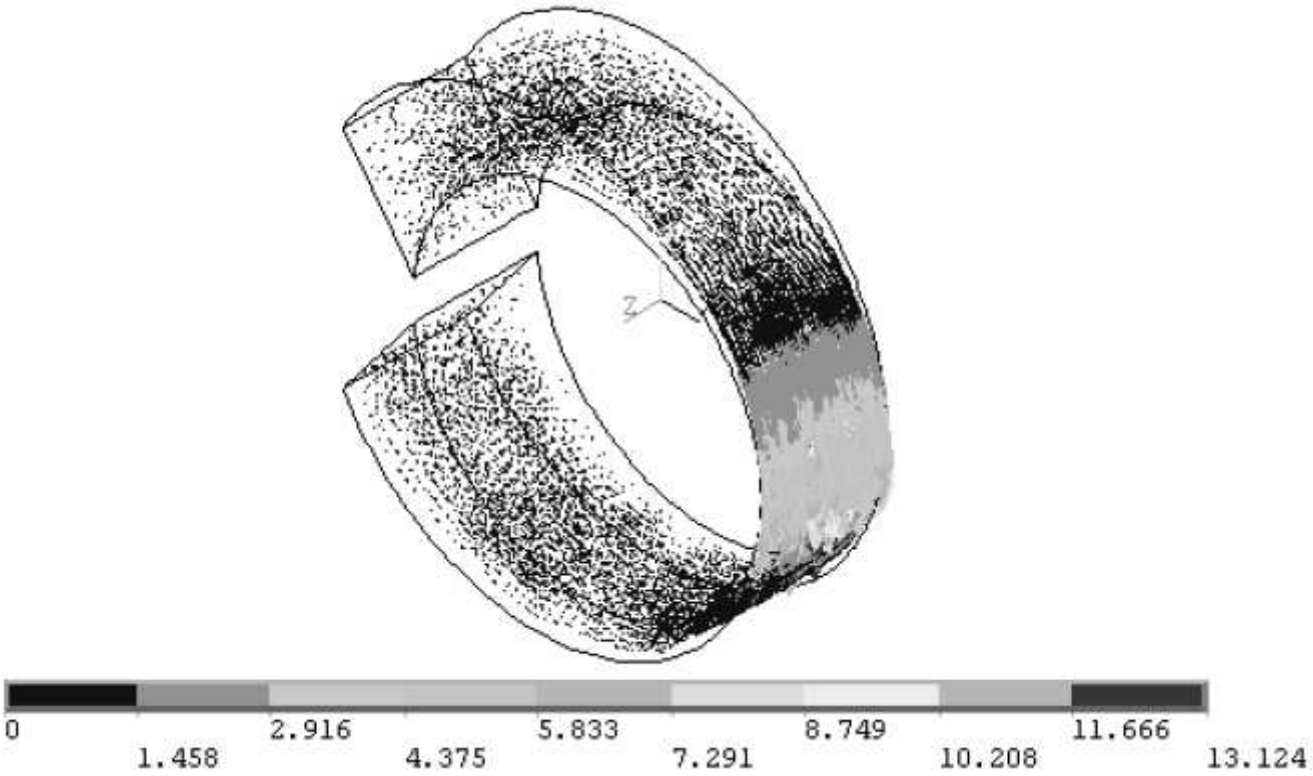

Figure 8

Stream wise sum velocity vector at Re = 550 in dye flow cell.

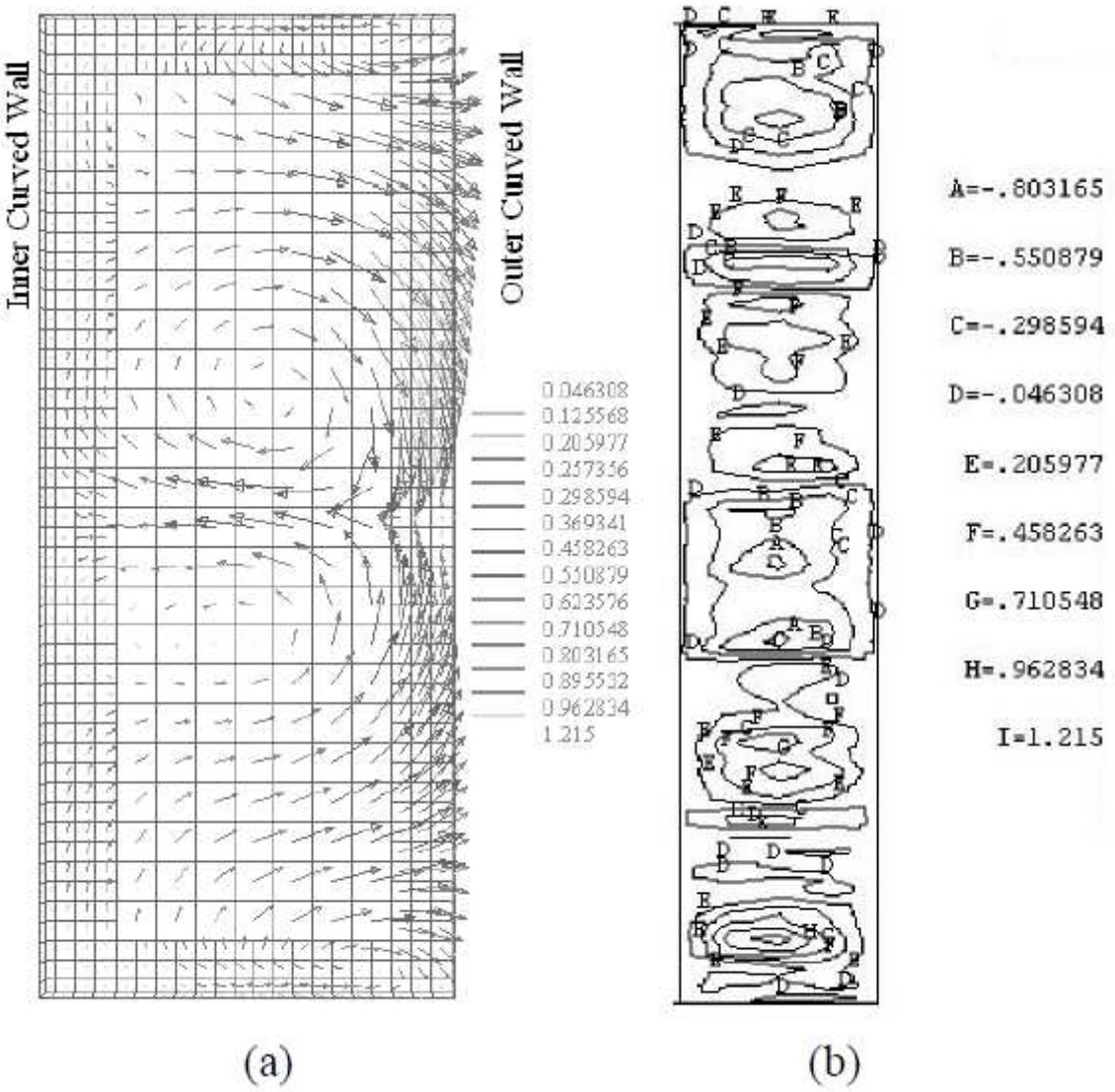

Figure 9

(a) Cross flow velocity vector and (b) resulting flow inhomogeneity at Re = 550 in dye flow cell at laser pump position

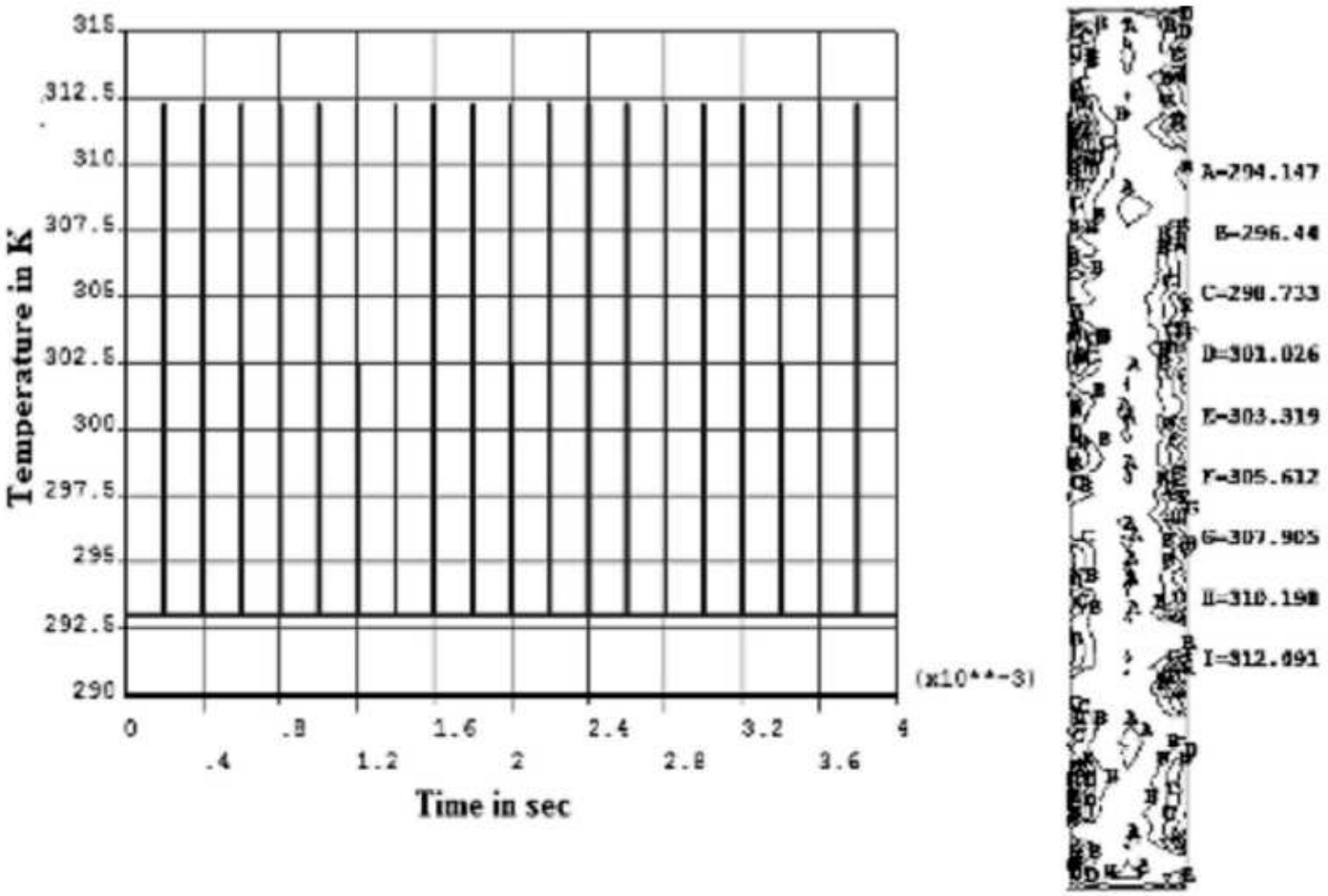

Figure 10

(a) Instantaneous temperature rise in dye gain medium with each pulse and (b) resulting temperature inhomogeiniety

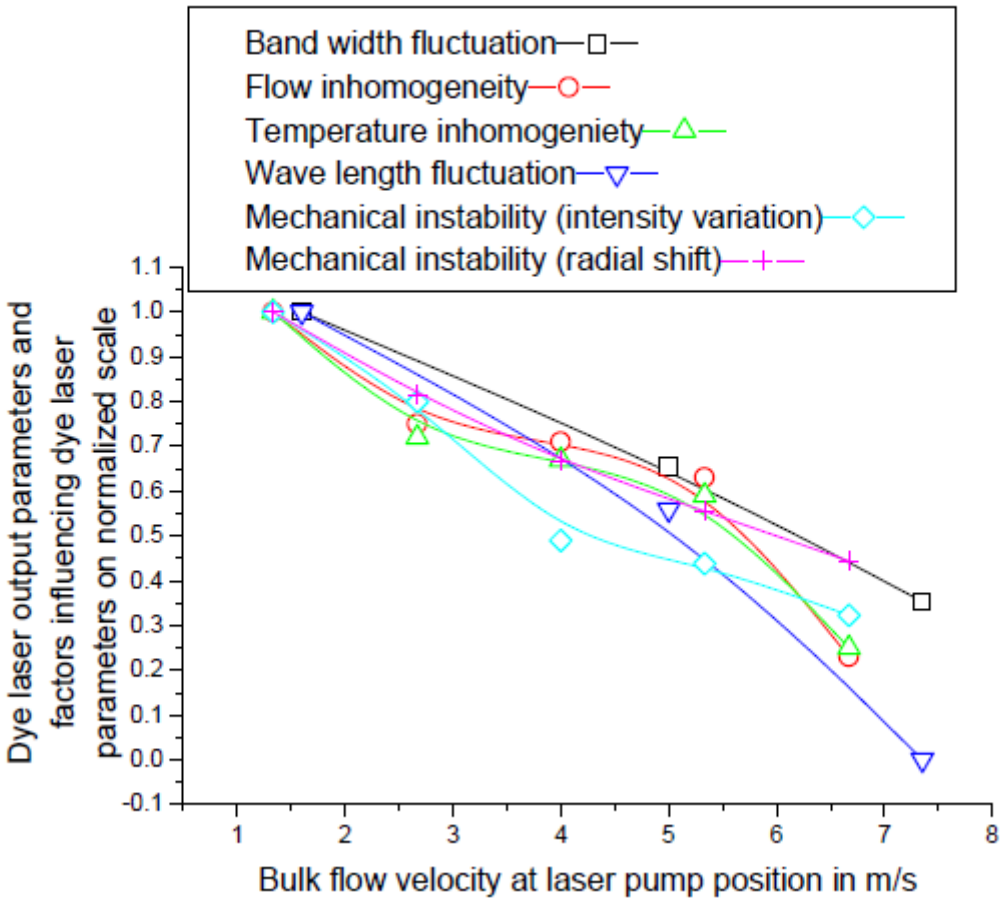

Figure 11

Variation of different parameters from test dye flow cell and comparison with dye laser output at different flow velocities at laser pump region.